Effects of gap fluctuations on the pair-transfer correlation function in nanometer-scale superconducting grains

R. Rossignoli,[1] N. Canosa,[1] and P. Ring[2]
[1]*Departamento de Física, Universidad Nacional de La Plata, C.C.67, La Plata (1900), Argentina*
[2]*Physik Department der Technischen Universität München, D-85747 Garching, Germany*
(Received 29 July 2002; revised manuscript received 26 November 2002; published 28 April 2003)

We investigate the effects of gap fluctuations on the pair-transfer correlation and spectral functions in nanoscopic superconducting grains at finite temperature, by means of the correlated static path approximation (CSPA). The present approach is able to provide a reliable description of the lowest energy weighted moments of the spectral function of small samples in critical regions, improving both the random-phase approximation (RPA) and the SPA predictions. The results confirm the persistence of pairing effects in the spectral function beyond the BCS critical temperatures and sizes, which is visible through the enhancement of the strength at low energies and the concomitant decrease in the normalized first energy moment. The role played by the zero and the imaginary quasiparticle RPA energies present in the CSPA is also discussed.

DOI: 10.1103/PhysRevB.67.144517 PACS number(s): 74.20.Fg, 74.25.Bt, 74.25.Fy

I. INTRODUCTION

Since the development of individual nanometer-scale aluminum grains by Ralph, Black, and Tinkham,[1,2] a great effort has been devoted to understand in detail the effects of superconducting pairing correlations in small electron systems.[3–13] Nanoscopic grains are characterized by a *discrete* energy spectrum, with a mean energy spacing between independent electron levels $\varepsilon \propto \hbar^2/mk_F V$ that can be of the same order as the bulk gap Δ_b. In these circumstances, the conventional BCS approximation, based on an independent quasiparticle picture, is not longer accurate. The higher-order correlations, which can be conveniently visualized as *fluctuations* of the pairing order parameter,[14] become increasingly important as the size decreases, i.e., as the ratio ε/Δ_b increases, and originate non-negligible pairing effects for temperatures, magnetic fields or sizes for which a superconducting BCS solution no longer exists. Accordingly, the BCS phase transitions become softened, and a smooth crossover to the so-called fluctuation dominated superconductivity regime ensues.[6,11] In the latter, pairing effects may become evident through observables other than a spectroscopic gap.[9,11,13]

One of the main signatures of pairing correlations is the enhancement of pair-transfer matrix elements. It is well known that the matrix element for Cooper pair transfer between superconducting ground states is strongly enhanced, being essentially proportional to the pairing order parameter Δ.[15,16] This will lead to a huge peak in the associated pair-transfer spectral function,[17,18] which is absent in a normal system. This quantity exhibits therefore a very high sensitivity to pairing correlations and can be used as an indicator of pairing effects in the fluctuation dominated regime. In nuclear physics, it has been employed to detect pairing effects in nuclei at high spin,[17] where superconductivity may become gapless[16] and hence it is hard to detect through direct observation of the spectrum. A recent exact calculation in small configuration spaces[18] indicates that evidences of pairing correlations should in principle, persist in this quantity for $T > T_c$ in small systems or for $\varepsilon > \Delta_b$ at low temperatures, which are visible through an enhancement of the strength at low energy $E - 2\mu$. Although a basic microscopic understanding of these effects in the fluctuation dominated regime can be achieved by means of the quasiparticle random-phase approximation (RPA),[18] which takes into account the small amplitude quantum fluctuations of Δ, this approach becomes unreliable in the vicinity of the BCS transition, where it develops divergencies associated with the onset of a zero energy mode.

The aim of this work is then to examine the adiabatic correlated static path approximation[19] (CSPA) to the pair-transfer spectral function, or more precisely, to its Laplace transform that is the imaginary time correlation function.[19] This quantity determines, through its derivatives, the energy weighted moments of the spectral function, and also exhibits a great sensitivity to pairing effects. The CSPA (Ref. 12) takes into account both the large amplitude static fluctuations of Δ (Ref. 14) plus the RPA correlations, and is known to provide an accurate approximation to the partition function in the crossover region around the critical temperature. As will be seen, the adiabatic CSPA approach is able to yield a simple smooth reliable description of the correlation function in critical regions, improving RPA results. It also provides a consistent treatment of the zero RPA modes, as well as of the complex modes that arise in the CSPA when the RPA is evaluated at a nonstationary mean field, above a low breakdown temperature. It should be mentioned that at low temperatures, where CSPA fails, exact canonical calculations for the standard discrete pairing Hamiltonian can be done, in principle, using Richardson's method for obtaining the exact eigenstates.[20,11] This method has been recently applied at zero temperature for evaluating thermodynamic properties[10] and correlation functions.[21] Nevertheless, its applicability at higher temperatures is limited in practice by the huge number of states involved in a thermal calculation as each excited state requires a separate evaluation. The CSPA provides then a simple alternative for finite temperatures. Improvements on the low-temperature limit of the CSPA have been recently also developed.[22]

In Sec. II, we describe the main features of the pair-transfer correlation function at finite temperature, including the independent quasiparticle approximation to this quantity and the adiabatic CSPA approach, in an ensemble with fixed number parity. The half-filled situation is discussed in detail. We also describe the standard and effective RPA approaches that can be obtained from the CSPA through a Gaussian approximation. Finite temperature results for parameters typical of nanometer scale grains are given in Sec. III, which include calculations with up to 1800 levels and comparison with full exact results for small configuration spaces. Finally, conclusions are drawn in Sec. IV.

II. THEORY

A. Pair-transfer correlation function

We consider a discrete pairing Hamiltonian of the form

$$\overline{H}=\sum_k (\varepsilon_k-\mu)N_k-GQ^\dagger Q, \tag{1}$$

$$N_k=c^\dagger_{k+}c_{k+}+c^\dagger_{k-}c_{k-}, \quad Q^\dagger=\sum_k \gamma_k c^\dagger_{k+}c^\dagger_{k-},$$

where $|k\pm\rangle$ denote time-reversed single-electron states with energies ε_k, $G>0$ is the pairing strength, γ_k are suitable weight factors, and the sums over k are restricted to a finite interval around the Fermi level μ. For $\gamma_k=1$, $Q^\dagger$ creates a standard Cooper pair.

Denoting with $|K\rangle$ the exact many-body eigenstates of Eq. (1), with $\overline{H}|K\rangle=\overline{E}_K|K\rangle$ and $\overline{E}_K=E_K-\mu N_K$, the imaginary time correlation function[19] for the operator $Q^\dagger$ can be defined as

$$G(\tau)\equiv\langle Q_{\overline{H}}(\tau)Q^\dagger\rangle=\sum_{K,K'} P_K|\langle K'|Q^\dagger|K\rangle|^2 e^{\tau(\overline{E}_K-\overline{E}_{K'})}, \tag{2}$$

where $Q_{\overline{H}}(\tau)=e^{\tau\overline{H}}Qe^{-\tau\overline{H}}$ and P_K is the initial statistical weight of state $|K\rangle$ ($\Sigma_K P_K=1$). Its Fourier transform in real time gives the spectral or strength function for pair transfer,[18]

$$S(E)=\frac{1}{2\pi i}\int_{-i\infty}^{i\infty} G(\tau)e^{\tau\overline{E}}d\tau$$

$$=\sum_{K,K'} P_K|\langle K'|Q^\dagger|K\rangle|^2\delta(\overline{E}-\overline{E}_{K'}+\overline{E}_K), \tag{3}$$

where $\overline{E}=E-2\mu$, while its derivatives at $\tau=0$ determine the energy weighted moments of $S(E)$,

$$M_n\equiv\int_{-\infty}^{\infty} S(E)\overline{E}^n dE=(-1)^n G^{(n)}(0). \tag{4}$$

For $n=0$, Eq. (4) yields the total strength

$$M_0=\int_{-\infty}^{\infty} S(E)dE=G(0)=\langle QQ^\dagger\rangle. \tag{5}$$

These expressions hold for *any* initial distribution P_K. In a grand canonical (GC) treatment at temperature $T=1/k\beta$ and fixed number parity (NP) $\nu=\pm1$,

$$P_K=\frac{1}{2}\mathcal{Z}^{-1}[1+\nu(-1)^{N_K}]e^{-\beta\overline{E}_K},$$

where $\mathcal{Z}=\mathrm{Tr}[\mathcal{P}_\nu e^{-\beta\overline{H}}]$, with $\mathcal{P}_\nu=\frac{1}{2}(1+\nu e^{i\pi N})$, is the GC partition function for fixed NP, and Eq. (2) becomes

$$G(\tau)=\mathcal{Z}^{-1}\mathrm{Tr}[\mathcal{P}_\nu e^{-(\beta-\tau)\overline{H}}Qe^{-\tau\overline{H}}Q^\dagger]. \tag{6}$$

B. Independent quasiparticle approximation

In a basic independent quasiparticle description, $\overline{H}$ is approximated by an operator of the form

$$\overline{h}=\sum_k \overline{\varepsilon}_k N_k-\Delta_k c^\dagger_{k+}c^\dagger_{k-}-\Delta^*_k c_{k-}c_{k+}, \tag{7}$$

in which case Eq. (6) becomes

$$G(\tau)=S_0+\sum_k S^+_k e^{-2\tau\lambda_k}+S^-_k e^{2\tau\lambda_k}, \tag{8}$$

where $\lambda_k=\sqrt{\overline{\varepsilon}^2_k+|\Delta^2_k|}$ are the quasiparticle energies and

$$S^\pm_k=\frac{e^{\pm\beta\lambda_k}\Gamma^{0\pm}_k}{2\sinh(\beta\lambda_k)}, \quad \Gamma^{0\pm}_k=\frac{1}{4}|\gamma^2_k|f_k\left(1\pm\frac{\overline{\varepsilon}_k}{\lambda_k}\right)^2,$$

$$S_0=\langle Q^\dagger\rangle\langle Q\rangle+\sum_{k,k'}\frac{\gamma^*_k\Delta_k\gamma_{k'}\Delta^*_{k'}}{4\beta\lambda_k\lambda_{k'}}\frac{\partial f_k}{\partial\lambda_{k'}}, \tag{9}$$

$$\langle Q^\dagger\rangle=\sum_k\frac{\gamma_k\Delta^*_k f_k}{2\lambda_k}=\langle Q\rangle^*, \tag{10}$$

$$f_k=\tanh\left(\frac{\beta\lambda_k}{2}\right)+\frac{2\nu\Gamma}{1+\nu\Gamma}\frac{1}{\sinh(\beta\lambda_k)}, \tag{11}$$

with $\Gamma=\Pi_k\tanh^2(\beta\lambda_k/2)$. The expressions for the full GC ensemble correspond to $\nu=0$ in Eq. (11). Here $S_0=\Sigma_K P_K|\langle K|Q^\dagger|K\rangle|^2$ contains the *diagonal* terms in Eq. (2), which arise in the present approximation when $\Delta_k\neq0$.[18] They represent the transitions between nearly degenerate states in the exact picture (i.e., between the superconducting ground states of the N and $N+2$ systems in an even grain at $T=0$), and are essential in the present description.[18] They account for a major fraction of the total strength $G(0)$ in the superconducting phase, practically exhausting $G(0)$ in a large system. The remaining terms in Eq. (8) correspond to absorption (S^+_k) and depletion (S^-_k) of quasiparticle pairs in excited states, the latter possibility arising at a finite temperature. The spectral function moments then become

$$M_n=S_0\delta_{n0}+\sum_k (2\lambda_k)^n[S^+_k+(-1)^n S^-_k]. \tag{12}$$

S_0 will not contribute to M_n for $n>0$. A decrease in the ratio M_1/M_0 is therefore a signature of pairing effects, indicating the concentration of the strength at low $\overline{E}$.

In a standard Hartree-like NP projected BCS approximation for Hamiltonian (1), $\overline{\varepsilon}_k=\varepsilon_k-\mu$ and $\Delta_k=\gamma_k\Delta$, with Δ determined by the self-consistent gap equation

$$\Delta=G\langle Q\rangle,\ \langle Q\rangle=\frac{1}{2}\,G\Delta\sum_k\,|\gamma_k^2|f_k/\lambda_k. \tag{13}$$

The diagonal term S_0 then becomes proportional to Δ^2. The transition to the normal phase at $T=T_c$ will be reflected in the vanishing of S_0 and hence in a sharp increase of the ratio M_1/M_0.

C. Gap fluctuations

Due to the effects of gap fluctuations, however, the previous BCS transitions are softened in small systems, and corrections to the BCS correlation function and moments become significant. The fluctuations of the pairing order parameter Δ can be rigorously introduced by means of the Hubbard-Stratonovich transformation and the ensuing path-integral representation of the partition function.[14] The CSPA partition function is obtained by conserving *large amplitude* static plus small amplitude quantum fluctuations of Δ and is given by[12]

$$\mathcal{Z}=\frac{2\beta}{G}\int_0^\infty e^{-\beta\mathcal{F}(\Delta)}C_{\rm RPA}(\Delta)\Delta\,d\Delta, \tag{14}$$

where

$$\mathcal{F}(\Delta)=\Delta^2/G-\beta^{-1}{\rm Tr}[\mathcal{P}_\nu\,e^{-\beta\overline{h}(\Delta)}], \tag{15}$$

$$\overline{h}(\Delta)=\sum_k\,\overline{\varepsilon}_kN_k-\Delta(Q^\dagger+Q)+h_0,$$

$$C_{\rm RPA}(\Delta)=\prod_k\,\frac{\omega_k}{2\lambda_k}\,\frac{\sinh(\beta\lambda_k)}{\sinh\left(\dfrac{\beta\omega_k}{2}\right)}, \tag{16}$$

with $\overline{\varepsilon}_k=\varepsilon_k-\mu-\frac{1}{2}G|\gamma_k^2|$, $h_0=\frac{1}{2}G\Sigma_k|\gamma_k^2|$, $\lambda_k=\sqrt{\overline{\varepsilon}_k^2+|\gamma_k^2|\Delta^2}$, and ω_k are the positive quasiparticle RPA energies around the running Δ, determined by the equation

$$\det[1+G\mathcal{R}(\omega,\Delta)]=0. \tag{17}$$

Here $\mathcal{R}(\omega,\Delta)$ is the finite temperature response matrix[18] for the operators $(Q_+,Q_-)=(Q^\dagger,Q)$ around $\overline{h}(\Delta)$,

$$\mathcal{R}_{\sigma\sigma'}(\omega,\Delta)=\sum_k\,f_k\left[\frac{(u_k^{\sigma'})^*u_k^\sigma}{\omega-2\lambda_k}-\frac{u_k^{-\sigma'}(u_k^{-\sigma})^*}{\omega+2\lambda_k}\right], \tag{18}$$

where $\sigma,\sigma'=\pm$, $u_k^+\equiv\gamma_ku_k^2$, $u_k^-\equiv-\gamma_k^*v_k^2$. The RPA energies ω_k can also be obtained as the eigenvalues of the associated RPA matrix.[12,13] The SPA partition function[14] is obtained by neglecting the RPA correction (16), and includes just the large amplitude static fluctuations of Δ around the BCS solution. The minimum of the potential (15) is determined precisely by the gap equation (13).

Equation (16) accounts for the small amplitude quantum fluctuations around the running Δ, and remains finite and positive for $\omega_k\to0$, as well as for imaginary ω_k provided $\beta|\omega_k|<2\pi\ \forall\ k,\Delta$. This condition determines the CSPA breakdown temperature $T_c^*<T_c$ below which the full CSPA is no longer applicable.[12]

Let us examine now the *adiabatic* CSPA approach to the correlation function,[19] where just transitions between states with the *same* order parameters (i.e., with the same Δ in the present situation) are considered. The final result, which can be formally obtained by the analytic continuation of the Fourier coefficients of $G(\tau)$ in the interval $[0,\beta]$, is essentially the average over Δ of the RPA correlation function plus a constant term. We obtain

$$G(\tau)=\int_0^\infty p(\Delta)G(\tau,\Delta)d\Delta, \tag{19}$$

where $p(\Delta)=(2\beta/G)e^{-\beta\mathcal{F}(\Delta)}C_{\rm RPA}(\Delta)\Delta/\mathcal{Z}$ and

$$G(\tau,\Delta)=S_0+\sum_k\,S_k^+e^{-\tau\omega_k}+S_k^-e^{\tau\omega_k}, \tag{20}$$

$$S_k^\pm=\frac{e^{\pm\beta\omega_k/2}\Gamma_k^\pm}{2\sinh\left(\dfrac{\beta\omega_k}{2}\right)}, \tag{21}$$

$$S_0=\frac{\Delta^2}{G^2}-\frac{1}{\beta G}-\sum_k\,\frac{\Gamma_k^++\Gamma_k^-}{\beta\omega_k}, \tag{22}$$

where the RPA strengths $\Gamma_k^\pm$ can be obtained from the RPA response function for $Q_+=Q^\dagger$,

$$R_{\rm RPA}(\omega,\Delta)=\{[1+G\mathcal{R}(\omega,\Delta)]^{-1}\mathcal{R}(\omega,\Delta)\}_{++}$$
$$=\sum_k\,\left[\frac{\Gamma_k^+}{\omega-\omega_k}-\frac{\Gamma_k^-}{\omega+\omega_k}\right]. \tag{23}$$

The CSPA moments in the adiabatic approach can then be expressed as

$$M_n=\int_0^\infty p(\Delta)M_n(\Delta)d\Delta, \tag{24}$$

$$M_n(\Delta)=S_0\delta_{n0}+\sum_k\,\omega_k^n[S_k^++(-1)^nS_k^-].$$

Equation (22) represents again the contribution of the diagonal elements, with the first two terms accounting for the Hartree contribution to $\langle QQ^\dagger\rangle$ [$(\beta G)^{-1}$ is just the average of Δ^2/G^2 in the absence of field ($Q=0$)]. The total CSPA strength M_0 agrees in this way with the average obtained from the CSPA partition function,

$$\frac{1}{\beta}\,\frac{\partial\ln\mathcal{Z}}{\partial G}=\langle Q^\dagger Q\rangle=M_0+\sum_k\,|\gamma_k^2|\langle N_k-1\rangle. \tag{25}$$

The SPA results correspond to the $G\to 0$ limit in Eq. (23), i.e., $\omega_k\to 2\lambda_k$, $\Gamma_k^{\pm}\to\Gamma_k^{0\pm}$, in which case Eqs. (19) and (24) become exactly the SPA average of Eqs. (8) and (12).[19] The most noticeable SPA effect in a small system is the subsistence of a nonvanishing diagonal term S_0 for $T>T_c$ due to the gap fluctuations.

In the CSPA, the sum in Eq. (20) is just the standard RPA correlation function for the running Δ. Note, however, that in the CSPA each RPA mode contributes in addition to the *diagonal* term S_0 through the last term in Eq. (22). This correction becomes particularly relevant when the lowest ω_k is close to zero, lowering the average of S_0 as compared with the SPA evaluation. This indicates a gradual replacement of the $\overline{E}=0$ strength by the lowest RPA mode as T increases above T_c. Moreover, this contribution becomes essential in the case of vanishing or imaginary RPA energies, as only the *complete* expression for $G(\tau,\Delta)$ and $M_n(\Delta)$ remain real and finite (above the CSPA breakdown), in contrast with the plain RPA term. This will be verified below for the half-filled case.

D. The symmetric half-filled case

Let us now analyze in more detail the symmetric half-filled case, dealing with levels ε_k located symmetrically with respect to the Fermi level, i.e., $\overline{\varepsilon}_{-k}=-\overline{\varepsilon}_k$, $\gamma_{-k}=\gamma_k$, where $k>0$ (<0) denotes here levels above (below) the Fermi level, such that $\lambda_{-k}=\lambda_k$, $f_{-k}=f_k$. In an even (odd) system, the chemical potential will lie halfway between the central levels (at the central level), so that $k=\pm 1,\pm 2,\ldots,\pm\Omega/2$ $(0,\pm 1,\ldots,\pm\Omega/2)$, with $\lambda_k\leqslant\lambda_{k+1}$ for $k\geqslant 0$. The total number of electrons is Ω $(\Omega+1)$. In the independent quasiparticle approximation, Eqs. (8) and (12) become

$$G(\tau)=S_0+\sum_k \Gamma_k^0\frac{\cosh\left[\left(\frac{\beta}{2}-\tau\right)2\lambda_k\right]}{\sinh[\beta\lambda_k]}, \tag{26}$$

$$M_n=S_0\delta_{n0}+\sum_k \Gamma_k^0(2\lambda_k)^n\begin{cases}\coth(\beta\lambda_k), & n \text{ even}\\ 1, & n \text{ odd},\end{cases}$$

with $\Gamma_k^0=\frac{1}{4}|\gamma_k^2|f_k(1+\alpha_k^2)$ and $\alpha_k=|\overline{\varepsilon}_k|/\lambda_k$. The SPA result is just the average over Δ of these expressions.

The RPA equation (17) can now be written as[18]

$$\prod_{\sigma=\pm 1}\left[1+2G\sum_k \frac{|\gamma_k^2|f_k\lambda_k\alpha_k^{1-\sigma}}{\omega^2-4\lambda_k^2}\right]=0, \tag{27}$$

so that the RPA energies will be the roots of each factor in Eq. (27). For nondegenerate levels ($\overline{\varepsilon}_k\neq\overline{\varepsilon}_{k'}$ if $k\neq k'$), each factor will possess in the even case $\Omega/2$ distinct roots ω_k^2, with the lowest one located below $4\lambda_1^2$ for $G>0$ and the rest between $4\lambda_{k-1}^2$ and $4\lambda_k^2$, whereas in the odd case the $\sigma=1$ factor will have an additional root $\omega_0^2<4\lambda_0^2$ due to the $k=0$ term (absent for $\sigma=-1$ as $\alpha_0=0$). All roots can then be labeled as ω_k, with $k\geqslant 0$ (<0) for those of the $\sigma=1$ (-1) factor.

In the symmetric case, Eq. (23) implies $\Gamma_k^{\pm}=\Gamma_k$ with

$$\Gamma_k=\frac{C_k}{\omega_k},\quad C_k^{-1}=8G^2\sum_{k'}\frac{|\gamma_{k'}^2|f_{k'}\lambda_{k'}\alpha_{k'}^{1-\sigma_k}}{[\omega_k^2-4\lambda_{k'}^2]^2}, \tag{28}$$

where $\sigma_k=1$ (-1) if $k\geqslant 0$ (<0). It can be verified that $\Gamma_k=-\frac{1}{2}\partial\omega_k/\partial G$, so that the total CSPA strength M_0 becomes identical to the CSPA average (25) (in the symmetric case $\Sigma_k|\gamma_k^2|\langle N_k-1\rangle=0$). The *total* contribution of each RPA mode to $G(\tau,\Delta)$ and $M_n(\Delta)$ becomes

$$G_k(\tau,\Delta)=\Gamma_k\left\{\frac{\cosh\left[\left(\frac{\beta}{2}-\tau\right)\omega_k\right]}{\sinh\left(\frac{\beta\omega_k}{2}\right)}-\frac{2}{\beta\omega_k}\right\}, \tag{29}$$

$$M_{nk}(\Delta)=\Gamma_k\omega_k^n\begin{cases}\coth\left(\frac{\beta\omega_k}{2}\right)-\delta_{n0}\frac{2}{\beta\omega_k}, & n \text{ even}\\ 1, & n \text{ odd}.\end{cases} \tag{30}$$

Note that the RPA correlations do not affect the first moment. It can be shown from Eq. (28) that $\Sigma_k\Gamma_k\omega_k=-\frac{1}{4}(\partial/\partial G)\Sigma_k\omega_k^2=\Sigma_k\Gamma_k^0(2\lambda_k)$ $\forall$ Δ, as $\Sigma_k\omega_k^2$ is the trace of the effective reduced RPA matrix.[18]

The lowest root ω_1 of the $\sigma=1$ factor is the "collective" mode, which for $T<T_c$ vanishes at the nonzero solution of Eq. (13), as can be seen from Eq. (27). In such a case, $\Gamma_1\to\infty$. Nonetheless, Eqs. (29)–(30) remain *finite* if $\omega_k\to 0$ for some k and Δ. In this limit,

$$G_k(\tau,\Delta)\to C_k\left[\frac{(\beta/2-\tau)^2}{\beta}-\frac{\beta}{12}\right]+O(\omega_k^2),$$

$$M_{0k}(\Delta)\to\frac{\beta C_k}{6},\quad M_{1k}(\Delta)=C_k,\quad M_{2k}(\Delta)\to\frac{2C_k}{\beta},$$

with C_k *finite* [Eq. (28)] and $M_{nk}(\Delta)\to 0$ for $n>2$. The zero mode will then provide a *finite* contribution to M_0, M_1, and M_2, while its contribution to higher moments vanishes. Note also that the $\sigma=-1$ term in Eq. (27) will also develop a zero root at a smaller gap determined by $G\Sigma_k|\gamma_k^2|f_k\alpha_k^2/2\lambda_k=1$, if T is sufficiently low.

For smaller values of Δ, ω_1 becomes purely imaginary ($w_1^2<0$, as seen in Fig. 1). Nonetheless, Eqs. (29)–(30) remain real and finite for ω_k imaginary if $\beta|\omega_k|\leqslant 2\pi$, i.e., above the CSPA breakdown. In such a case, since $C_k>0$, Eq. (30) becomes

$$|\Gamma_k\omega_k|^n\begin{cases}(-)^{n/2}\left[\delta_{n0}\frac{2}{\beta|\omega_k|}-\cot\frac{\beta|\omega_k|}{2}\right], & n \text{ even}\\ (-)^{(n-1)/2}, & n \text{ odd}.\end{cases}$$

It can be seen that $M_{0k}(\Delta)>0$, so that an imaginary ω_k provides a *positive* contribution to the CSPA strength. Its contribution to higher moments can nevertheless be negative. Even contributions diverge for $\beta|\omega_k|\to 2\pi$.

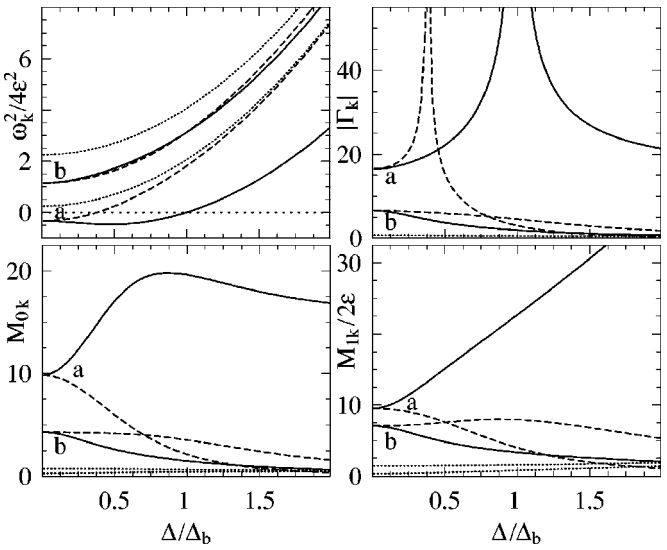

FIG. 1. Top: The square of the four lowest quasiparticle RPA energies (left) and the corresponding strengths (28) (right) as a function of Δ, for size parameter $\xi=\varepsilon/\Delta_b\approx 0.74$, at $T=0.5T_c$. Full (dashed) lines depict the first two roots (a and b) of the $\sigma=+1$ (-1) factor in Eq. (27). Dotted lines depict for reference the first two quasiparticle pair squared energies $(2\lambda_k)^2$ (left) and strengths (right). Bottom: The corresponding contributions to the total strength (left) and the first energy moment of the spectral function (right). Δ_b and T_c denote the bulk gap and critical temperature.

E. Standard and effective Gaussian approximations

The CSPA derived quasiparticle RPA approximation to $G(\tau)$ is, in principle, given by Eq. (20), evaluated at the self-consistent gap Δ_0 that minimizes $\mathcal{F}(\Delta)$. However, in order to obtain a more accurate evaluation of the diagonal term S_0 (and hence of the total strength M_0), it is preferable to evaluate Eq. (14) in the Gaussian approximation around Δ_0 and determine M_0 through Eq. (25). We may then recover S_0 as

$$S_0 = M_0 - \sum_k (S_k^+ + S_k^-),$$

such that $G(0)=M_0$.

For $T>T_c$, a gaussian approximation to Eq. (14) around $\Delta_0=0$ leads to[12]

$$\mathcal{Z}\approx e^{-\beta\mathcal{F}(0)}\prod_k \frac{\sinh(\beta|\overline{\varepsilon_k}|)}{\sinh\left(\frac{\beta\omega_k}{2}\right)}, \tag{31}$$

where $e^{-\beta\mathcal{F}(0)}$ is just the normal partition function and ω_k are the RPA energies for $\Delta=0$. In the half-filled case, Eqs. (31) and (25) yield $M_0=\Sigma_k\Gamma_k\coth(\beta\omega_k/2)$, implying $S_0=0$ and

$$G(\tau)=\sum_k \Gamma_k \frac{\cosh\left[\left(\frac{\beta}{2}-\tau\right)\omega_k\right]}{\sinh\left(\frac{\beta\omega_k}{2}\right)}. \tag{32}$$

For $T<T_c$, a similar procedure around the solution $\Delta_0\neq 0$ of Eq. (13) yields

$$\mathcal{Z}\approx e^{-\beta\mathcal{F}(\Delta_0)}C_{\mathrm{RPA}}(\Delta_0)\frac{\Delta_0}{G}\left[\frac{8\pi\beta}{\mathcal{F}''(\Delta_0)}\right]^{1/2}, \tag{33}$$

$$\mathcal{F}''(\Delta)=\frac{2}{G}-\sum_k \frac{|\gamma_k^2|}{\lambda_k}\left(f_k\alpha_k^2+\Delta\frac{\partial f_k}{\partial\Delta}\right). \tag{34}$$

In the half-filled case, we then obtain

$$G(\tau)=M_0+\sum_k \Gamma_k\left[\frac{\cosh\left[\left(\frac{\beta}{2}-\tau\right)\omega_k\right]}{\sinh\left(\frac{\beta\omega_k}{2}\right)}-\coth\left(\frac{\beta\omega_k}{2}\right)\right], \tag{35}$$

where M_0 is determined by Eqs. (33) and (25) and ω_k are the RPA energies for $\Delta=\Delta_0$. The lowest RPA energy now vanishes, but Eq. (35) remains finite for $T<T_c$ [if $\omega_k\to 0$, the corresponding term in Eq. (35) becomes $C_k\tau(\tau-\beta)/\beta$, leading to $M_{0k}=0$ and the same previous expressions $M_{1k}=C_k$, $M_{2k}=2C_k/\beta$, and $M_{nk}=0$, if $n\geq 3$].

Equations (31)–(33) provide an accurate approximation to $\mathcal{Z}$ and M_0 away from T_c, but *diverge* for $T\to T_c$ [as $\mathcal{F}''(0)=0$ at $T=T_c$] failing therefore in the crossover region around T_c. In the previous scheme, the influence of the measure Δ in $p(\Delta)$ was neglected when determining the expansion point Δ_0. This factor arises from the original two-dimensional integral [the gauge angle has been integrated out in Eq. (14)] and represents and effective multiplicity of the ''intrinsic'' partition function,[23] accounting for its reorientations in the gauge space. It is possible to improve the Gaussian approximation in the critical region in a simple way just by taking into account the effect of Δ on the potential.[12] The new expansion point is determined from the minimization of the effective potential $\tilde{\mathcal{F}}(\Delta)=\mathcal{F}(\Delta)-\beta^{-1}\ln\Delta/G$, which leads to the equation

$$1=\frac{1}{2}G\left[\sum_k |\gamma_k^2| f_k/\lambda_k + 1/(\beta\Delta^2)\right], \tag{36}$$

whose solution $\tilde{\Delta}_0>\Delta_0$ remains nonzero for all $T>0$. The ensuing approximation to Eq. (14) has the same form (33), with $\Delta_0\to\tilde{\Delta}_0$ and $\mathcal{F}''(\Delta_0)\to\tilde{\mathcal{F}}''(\tilde{\Delta}_0)$. The result remains finite and smooth throughout the crossover region, including $T=T_c$, and approaches Eqs. (31)–(33) away from T_c.

III. RESULTS

We consider in what follows the widely employed, uniformly spaced model,[11] where a constant spacing $\varepsilon_k-\varepsilon_{k-1}=\varepsilon$ is assumed and pairing is restricted to an energy band of

width $2\omega_c=\Omega\varepsilon$ around the Fermi level [with $\gamma_k=1$ (0) if $|\varepsilon_k-\mu|<\omega_c$ $(>\omega_c)$]. We set the coupling strength $G=g\varepsilon$, with $g=0.2$ (assumed size independent). The relevant size parameter is the spacing to bulk gap ratio $\xi=\varepsilon/\Delta_b$, where $\Delta_b=2\omega_c e^{-1/g}$ is the solution of Eq. (13) in the bulk limit $\varepsilon\to 0$ (i.e., $\xi\ll 1$) for weak coupling. The bulk critical temperature is $T_c=\alpha\Delta_b$, with $\alpha=e^{\gamma}/\pi\approx 0.567$ (γ is the Euler's constant).

Nanometer-scale grains may possess size parameters of order one or even larger. In the present model, Eq. (13) predicts a parity dependent lower-size limit for superconductivity,[3,4] namely $\xi_c^+\approx 3.56$, $\xi_c^-\approx 0.89$ for an even and odd grain, respectively, such that for $\xi>\xi_c^{\nu}$ no superconducting solution of Eq. (13) exists at $T=0$. Nevertheless, for these sizes gap fluctuations become very important. The gap fluctuation in the SPA is of the order[13] of $\langle\Delta^2\rangle\approx\Delta_b^2\xi\alpha t/\ln t$ for $t\equiv T/T_c>1$ (and $T\ll\omega_c$), approaching the same order as Δ_b^2 for $\xi\sim 1$. Moreover, it has been shown[10] that neither BCS nor perturbative methods are accurate at $T=0$ in the intermediate regime $\varepsilon\lesssim\Delta_b\lesssim\sqrt{\omega_c\varepsilon}$, i.e., $\Delta_b/\omega_c\lesssim\xi\lesssim 1$, where $\Delta_b/\omega_c=2e^{-1/g}$ (≈ 0.013 for $g=0.2$).

We first depict in Fig. 1 the typical behavior with Δ of the four lowest RPA energies [the first two roots of each factor in Eq. (27)] for $T<T_c$, together with their contribution to the first moments. We have chosen an even case with $\Omega=200$ levels ($\xi\approx 0.74$) at $T=0.5T_c$, in which the self-consistent gap is $\Delta_0\approx 0.996\Delta_b$. The lowest RPA energy ω_1 vanishes at $\Delta=\Delta_0$, becoming imaginary for $\Delta<\Delta_0$ and remaining considerably smaller than the quasiparticle pair energy $2\lambda_1$ for $\Delta>\Delta_b$. The corresponding strength Γ_1 is therefore very large and diverges at $\Delta=\Delta_0$. The lowest root of the $\sigma=-1$ factor becomes also imaginary for $\Delta<\Delta_0'\approx 0.38\Delta_b$, but approaches $2\lambda_1$ above this value. The corresponding strength, although diverging at Δ_0', becomes accordingly much smaller than Γ_1 for $\Delta>\Delta_b$, approaching the unperturbed value. The remaining RPA energies are real for all Δ and their strengths, even though larger than the unperturbed values, remain much smaller than Γ_1. As seen in the lower panels, the lowest RPA mode provides the main contribution to the total RPA strength and a significant contribution to the first energy moment for $\Delta\sim\Delta_b$, although the contribution from the other modes are also important and larger than the unperturbed values. Note that all contributions remain finite and smooth for all Δ.

Figure 2 depicts the scaled total strength m_0 and the normalized first energy moment m_1 and quadratic dispersion m_2 (all dimensionless), defined by

$$m_0\equiv\frac{\varepsilon}{\omega_c}M_0,\quad m_1\equiv\frac{1}{\omega_c}\frac{M_1}{M_0},\tag{37}$$

$$m_2\equiv\frac{3}{\omega_c^2}\left[\frac{M_2}{M_0}-\frac{M_1^2}{M_0^2}\right],\tag{38}$$

for decreasing sizes $\xi\approx 0.08$, 0.25, and 0.74, corresponding to $\Omega=1800$, 600, and 200 levels, respectively, in the even system (note that the corresponding total number of many-body states in the canonical ensemble are $\approx 7\times 10^{1081}$, 4×10^{359} and 10^{119}). The scaling factors in Eqs. (37)–(38) have been chosen such that in the normal (nonsuperconducting) case all $m_i\to 1$ for $T,\varepsilon\ll\omega_c$, so that the BCS result for $T>T_c$ is approximately 1. The deviation from this asymptotic value will therefore reflect the effects from the gap fluctuations. All cases correspond to the intermediate regime,[10] $\Delta_b/\omega_c<\xi<1$. RPA denotes here results obtained from the approximations (32) and (35), and diverge accordingly at $T=T_c$. For $T>T_c$ they are practically coincident for the different sizes considered, so that only a single RPA curve is seen. The CSPA results remain smooth in the critical region, and approach those of RPA away from T_c. The CSPA breakdown occurs at $T/T_c\approx(0.29,0.3,0.31)$ in the even case and $\approx(0.29,0.27,0.18)$ in the odd case for $\xi\approx$ 0.08, 0.25, and 0.74, respectively.

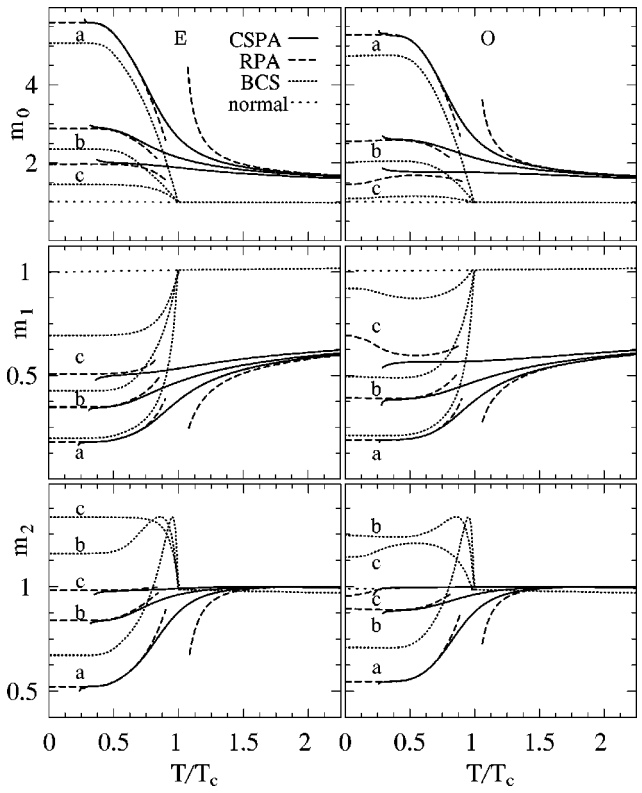

FIG. 2. The scaled total strength (top), and the normalized first energy moment (center) and dispersion (bottom) of the pair-transfer spectral function, Eqs. (37)–(38) (dimensionless), in an even (left) and odd (right) grain for size parameters $\xi\approx 0.08$ (case *a*), 0.25 (case *b*), and 0.74 (case *c*) (corresponding to $\Omega=1800$, 600, and 200 levels in the even system), according to NP projected CSPA, RPA, and BCS results. The normal result for $T<T_c$ is also depicted.

In a large superconductor, $M_0\approx\Delta_b^2/G^2=(g\xi)^{-2}$ at $T=0$ for $\xi\ll 1$, so that $m_0\approx\Delta_b/(\omega_c\xi g^2)$. Accordingly, as size decreases, m_0 decreases for $T\lesssim T_c$, although the decrease in the CSPA is less pronounced than in the BCS approximation. For $T>T_c$, the CSPA results for m_0 remain larger than the normal value, and become almost size independent for T well above T_c, approaching the present RPA result. Thus,

the enhancement of the total strength for $T \gg T_c$ can be ascribed to the RPA correlations contained in the correction factor of Eq. (31).

In a large sample, the increase in the strength for $T < T_c$ is accompanied by a strong decrease in m_1, which reflects the appearance of the collective peak at $\bar{E} \approx 0$ (in an exact canonical calculation, it actually appears at $\bar{E} \approx \varepsilon = \xi \Delta_b$.[18]) In BCS, it can be seen that M_1 is of the order of $\omega_c^2 / \xi \Delta_b$ at $T = 0$ for $\xi \ll 1$, in which case $m_1 \sim 1/m_0 \approx \xi g^2 \omega_c / \Delta_b$. As size decreases, the drop of m_1 for $T < T_c$ becomes less pronounced, although the CSPA result becomes increasingly smaller than the BCS value. For $T > T_c$, the CSPA result is significantly smaller than the normal value for all sizes, and depends again only weakly on the size ξ for $T \gg T_c$. This indicates that an appreciable enhancement of the strength at low $\bar{E}$ remains for $T > T_c$.

The normalized quadratic dispersion m_2, which is a global measure of the width of the spectral function, exhibits again a significant drop for $T < T_c$ in large samples (in BCS, m_2 is again of order $\sim 1/m_0$ at $T = 0$ for $\xi \ll 1$). As the grain size decreases, this drop becomes less pronounced in the CSPA, whereas in BCS m_2 may become at low temperatures even larger than the normal value. Moreover, the BCS result exhibits a pronounced peak in large samples just before the transition, which is, however, totally absent in the CSPA. In contrast, very small deviations from the normal value take place for $T > T_c$ in all approximations and sizes for this value of g.

The CSPA results for the odd grain are similar. The total CSPA strength is slightly smaller than in the even case, reflecting weaker pairing correlations, and m_1 and m_2 are therefore slightly larger than the corresponding even values. Nevertheless, the parity dependence of the CSPA results is much weaker than in BCS. For size c, which is already close to the BCS lower size limit ξ_c^-, the BCS result for $T < T_c$ differs considerably from that of the even case, although this effect is not seen in the concomitant CSPA result. The total strength exhibits initially in BCS and RPA a slight increase with temperature in small samples (as the particle lying at the Fermi level becomes able to move to higher levels), which lead in turn to a flat minimum in m_1. This effect could not be corroborated by the CSPA results since it occurs for temperatures close to the CSPA breakdown.

It should be mentioned that results in the present model depend on both the size parameter ξ and g (i.e., on ξ and Δ_b / ω_c). Nevertheless, within the weak-coupling regime, the behavior with size and temperature of the previous quantities for other values of g are similar to those in Fig. 2. At fixed ξ, the deviation of m_0, m_1, and m_2 from the normal result increases as g increases and, in particular, the CSPA result for the dispersion m_2 may be smaller than the normal value for $T > T_c$. On the other hand, for $T > T_c$ the CSPA and RPA results for m_0 and m_1 deviate from the normal result even if $\xi < \Delta_b / \omega_c$. RPA correlations are then essential for describing these scaled quantities even in this region.

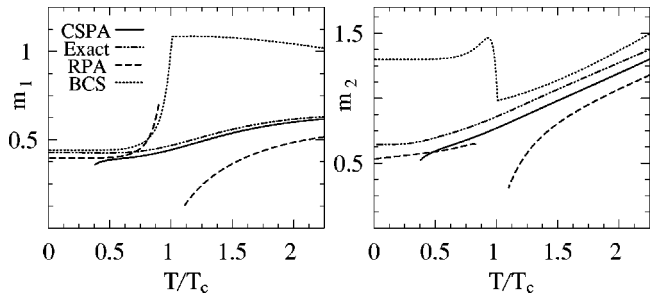

FIG. 3. Comparison between exact and approximate results for the normalized first energy moment and dispersion in an even case with $\Omega = 10$ and $\xi \approx 0.74$.

CSPA results for m_1 and m_2 are theoretically confirmed in Fig. 3, where comparison with *exact* thermal NP projected GC results for a small configuration space ($\Omega = 10$ levels), obtained with the exact eigenvalues of the Hamiltonian (1) at effective size parameter $\xi \approx 0.74$ (corresponding to $g = 0.5$), is made. The results differ from those of case c in Fig. 2 due to the larger ratio Δ_b / ω_c. Above the breakdown temperature $T/T_c \approx 0.31$, the adiabatic CSPA results are in close agreement with the exact ones, which remain totally smooth at $T = T_c$ and show no evidence of the peak in m_2 displayed by BCS. A similar agreement is obtained for the other size parameters of Fig. 2 and for odd grains. Note also that there is a good agreement between the exact and the RPA results for $T \ll T_c$, if ξ is not close to ξ_c.

The plain SPA results for these quantities deviate considerably from those of the CSPA, particularly for the dispersion m_2, as seen in Fig. 4 for the even case b of Fig. 2 ($\Omega = 600$), indicating the important role played by RPA correlations. On the other hand, the results obtained with the *effective* RPA approximation determined by Eq. (36) are in remarkable close agreement with the full CSPA results for both m_1 and m_2 at all temperatures, except for a narrow interval around T_c, where it exhibits a small bump, remaining nevertheless finite at $T = T_c$. A similar agreement for these quantities is found for the other cases in Fig. 2, as well as for the ultrasmall sizes considered in Fig. 6. It provides therefore a much better gaussian evaluation of Eq. (14) in finite systems, in all regimes, in comparison with the conventional approximations (31)–(33).

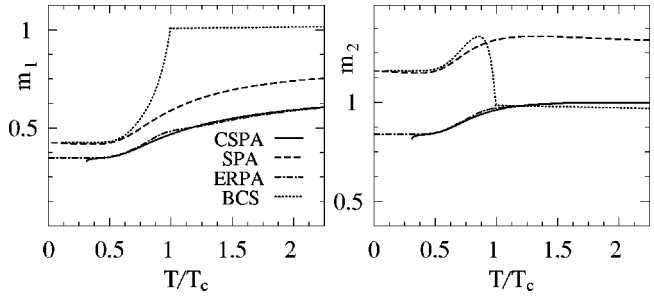

FIG. 4. The normalized first energy moment and dispersion for the even case b of Fig. 2, according to NP projected CSPA, SPA, effective RPA, and BCS results.

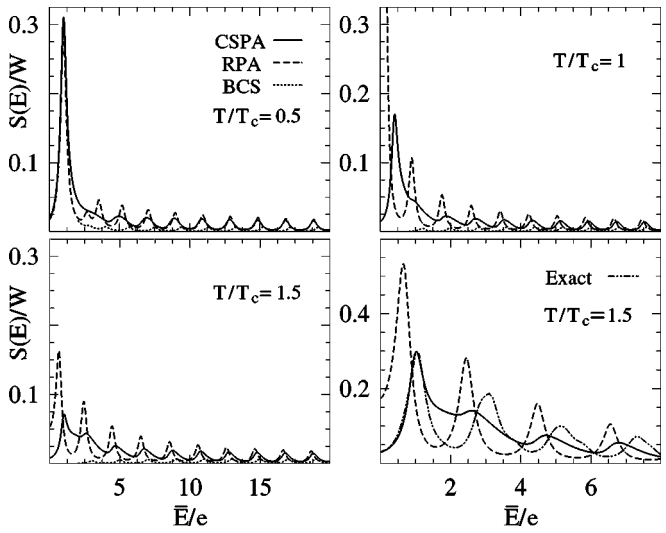

FIG. 5. The pair-transfer spectral function for the even case *c* of Fig. 2, and increasing temperatures, according to NP projected CSPA, RPA, and BCS results (in units of ε^{-1}). The right bottom panel shows a comparison with exact results for the parameters of Fig. 3.

Figure 5 depicts results for the pair-transfer spectral function for the even case *c* in Fig. 2. Details about conventional RPA and BCS results for this quantity have been discussed in Ref. 18. We have set a width $\eta=0.25\varepsilon$ for the representation of the δ functions.[18] For $T<T_c$ (top left panel), the peak arising from the diagonal term S_0 (which we have here located at $\bar{E}\approx\varepsilon$, according to the exact results and the canonical energy correction[18]) is clearly dominant and CSPA corrections to the RPA results are small. Nevertheless, for $T\approx T_c$, where the RPA result diverges at $\bar{E}=0$, the CSPA strength remains finite, in agreement with the exact behavior, and is significantly larger than the already normal BCS results. For $T>T_c$, the CSPA strength at low $\bar{E}$ is lower and more spread than in the RPA, although the enhancement over the BCS results remains significant. The RPA results overestimate the strength at low $\bar{E}$ for T close to T_c,[18] as seen in the right bottom panel where the comparison with exact NP projected GC thermal results for the parameters of Fig. 3 is made. CSPA improves RPA, although the agreement with the exact spectral function is only qualitative, in spite of the good prediction of the first energy weighted moments (Fig. 3). We should mention that results obtained with the effective RPA approach determined by Eq. (36) (not shown) also improve those of the conventional RPA, but differ from those of the full CSPA as fluctuations of the RPA energies are not included. The ensuing peaks are hence narrower and similar to those of the conventional RPA.

Finally, Fig. 6 depicts the behavior of m_1 for $g=0.2$ and $\xi\approx1.5$ (case *d*), with $\Omega=100$, as well as for the *ultrasmall* sizes $\xi\approx3.7$ (case *e*) and $\xi\approx15$ (case *f*), for which BCS is already normal for all *T*. The temperature is now in units of the spacing ε. The CSPA result remains smaller than the normal result even for size *f*, indicating the persistence of pairing effects. For this size we have also calculated the exact thermal result that lies quite close to the CSPA result except for $T\to0$. It is also seen that when ξ is close to the even critical size ξ_c^+, as in case *e*, the RPA result ceases to be accurate at low temperatures, becoming too small, which reflects the RPA overestimation of the strength at low $\bar{E}$.[18] CSPA improves RPA results at low temperature for cases *e* and *f* (where there is no CSPA breakdown), although it approaches the RPA results for $T\to0$.

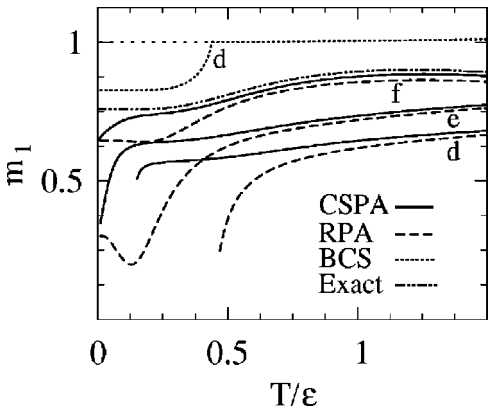

FIG. 6. The normalized first energy moment for $\xi\approx1.5$ (case *d*), 3.7 (case *e*) and 15 (case *f*) in the even grain, according to NP projected CSPA, RPA, and BCS results. The exact result for the ultrasmall case *f* is also depicted. The sparse dotted line indicates the normal result.

IV. SUMMARY

The present adiabatic CSPA treatment of the pair-transfer correlation function is able to provide a simple yet reliable description of the lowest energy weighted moments of the spectral function at finite temperature, significantly improving BCS and RPA results in the crossover region around T_c. It also gives a fully consistent treatment of the zero and the imaginary RPA energies above the CSPA breakdown without singularities. For the half-filled case, we have explicitly shown that the zero mode provides a finite contribution to the total strength and the two first energy moments. However, in order to achieve a closer agreement with the spectral function, higher-order corrections are necessary, which should include nonadiabatic effects at higher temperatures as well particle number projection at low temperatures. Nonetheless, the present approach is sufficient to confirm the enhancement of the pair-transfer strength at low energies $\bar{E}$ beyond the BCS critical temperature or sizes, which constitutes a clear evidence of the persistence of pairing effects.

ACKNOWLEDGMENTS

R.R. and N.C. acknowledge support from CIC and CONICET, respectively, of Argentina, and a grant of Fundación Antorchas. They are grateful to the hospitality of the Physik Department der Technischen Universität München, where part of this work was done.

[1] D.C. Ralph, C.T. Black, and M. Tinkham, Phys. Rev. Lett. **74**, 3241 (1995).
[2] C.T. Black, D.C. Ralph, and M. Tinkham, Phys. Rev. Lett. **76**, 688 (1996); D.C. Ralph, C.T. Black, and M. Tinkham, *ibid.* **78**, 4087 (1997).
[3] R.A. Smith and V. Ambegaokar, Phys. Rev. Lett. **77**, 4962 (1996); B. Jankó, A. Smith, and V. Ambegaokar, Phys. Rev. B **50**, 1152 (1994).
[4] J. von Delft, A.D. Zaikin, D.S. Golubev, and W. Tichy, Phys. Rev. Lett. **77**, 3189 (1996).
[5] K.A. Matveev and A.I. Larkin, Phys. Rev. Lett. **78**, 3749 (1997).
[6] F. Braun and J. von Delft, Phys. Rev. Lett. **81**, 4712 (1998); F. Braun and J. von Delft, Phys. Rev. B **59**, 9527 (1999).
[7] R. Balian, H. Flocard, and M. Vénéroni, Phys. Rep. **317**, 251 (1999).
[8] A. Mastellone, G. Falci, and R. Fazio, Phys. Rev. Lett. **80**, 4542 (1998).
[9] A. Di Lorenzo, R. Fazio, F.W.J. Hekking, G. Falci, A. Mastellone, and G. Giaquinta, Phys. Rev. Lett. **84**, 550 (2000).
[10] M. Schechter, Y. Imry, Y. Levinson, and J. von Delft, Phys. Rev. B **63**, 214518 (2001).
[11] J. von Delft and D.C. Ralph, Phys. Rep. **345**, 61 (2001).
[12] R. Rossignoli, N. Canosa, and P. Ring, Ann. Phys. (N.Y.) **275**, 1 (1999); Phys. Rev. Lett. **80**, 1853 (1998).
[13] N. Canosa and R. Rossignoli, Phys. Rev. B **62**, 5886 (2000); R. Rossignoli and N. Canosa, *ibid.* **63**, 134523 (2001).
[14] B. Mühlschlegel, D.J. Scalapino, and R. Denton, Phys. Rev. B **6**, 1767 (1972).
[15] P. Ring and P. Schuck, *The Nuclear Many-Body Problem* (Springer, New York, 1980), Chap. 11; S.Y. Chu, J.O. Rasmussen, M.A. Stoyer, L.F. Canto, R. Donangelo, and P. Ring, Phys. Rev. C **52**, 685 (1995).
[16] A. Bohr and B. R. Mottelson, *Nuclear Structure* (Benjamin, New York, 1985), Vol. II.
[17] J.L. Egido and J.O. Rasmussen, Phys. Rev. C **36**, 316 (1987).
[18] R. Rossignoli, N. Canosa, and J.L. Egido, Phys. Rev. B **64**, 224511 (2001).
[19] R. Rossignoli and P. Ring, Nucl. Phys. A **633**, 613 (1998).
[20] R.W. Richardson, Phys. Lett. **3**, 277 (1963); R.W. Richardson and N. Sherman, Nucl. Phys. **52**, 221 (1963).
[21] L. Amico and A. Osterloh, Phys. Rev. Lett. **88**, 127003 (2002).
[22] C. Rummel and J. Ankerhold, Eur. Phys. J. B **29**, 105 (2001).
[23] R. Rossignoli, N. Canosa, and P. Ring, Phys. Rev. Lett. **72**, 4070 (1994).